Volatile organic compound removal over bentonite-supported Pt, Mn and Pt/Mn monolithic catalysts

**J. Esteban Colman-Lerner · Miguel A. Peluso ·
Jorge E. Sambeth · Horacio J. Thomas**

Abstract The catalytic oxidation of volatile organic compounds (VOCs) (ethanol and toluene) alone and in mixture was investigated over Pt, Mn and Pt/Mn impregnated bentonite monoliths. Their properties were characterized by using the Brunauer–Emmett–Teller method, X-ray diffraction, X-ray photoelectron spectra and temperature programmed reduction (TPR). Independently of which catalyst was used, ethanol was more easily oxidized than toluene. In toluene oxidation, the sequence of catalytic activity was as follows: Pt/Mn/B > Pt/B > Mn/B, probably due to some favorable synergetic effects between Pt and Mn and to the presence of Mn^{3+}/Mn^{4+} species. In ethanol oxidation, Pt/Mn/B and Pt/B present similar activities, and greater than that of Mn/B. In the VOC mixture, toluene slows down the partial oxidation of ethanol towards acetaldehyde. On the contrary, the presence of ethanol has a promoting effect on toluene oxidation.

Keywords Bentonite · VOCs mixtures · MnO_x · Pt

J. E. Colman-Lerner · M. A. Peluso (✉) · J. E. Sambeth · H. J. Thomas
Centro de Investigación y Desarrollo en Ciencias Aplicadas "Dr. Jorge J. Ronco", CONICET CCT
La Plata, UNLP, 47 N° 257, 1900 La Plata, Argentina
e-mail: apelu@quimica.unlp.edu.ar

J. E. Colman-Lerner · M. A. Peluso · J. E. Sambeth
Facultad de Ciencias Exactas, UNLP, 47 and 115, 1900 La Plata, Argentina

J. E. Colman-Lerner
Centro de Investigaciones del Medio Ambiente (CIMA), Facultad de Ciencias Exactas, UNLP,
47 y 115, 1900 La Plata, Argentina

H. J. Thomas
Planta Piloto Multipropósito PLAPIMU, CICPBA-UNLP, C. Centenario and 506,
M. B. Gonnet, Argentina

Introduction

Volatile organic compounds (VOCs) are considered as significant atmospheric pollutants not only for their toxicity and malodorous nature, but also because they are ozone and smog precursors [1]. Catalytic oxidation can be considered an effective way for reducing the emissions of VOCs from stationary sources [2–4]. Supported platinum and palladium are the most commonly used catalysts [5, 6]. Nevertheless, the development of transition metal oxides for catalytic combustion has been widely reported in the literature [7–10], because they are cheaper than noble metals.

For practical applications regarding VOC oxidation, the catalyst should be supported on a structured support to treat large gas flows with low pressure drop. The most widely used structured supports are the honeycomb monoliths made of ceramic or metallic materials [11].

Manganese oxide and platinum supported on metallic or ceramic monoliths are widely employed in the combustion of single VOCs [12–15].

In practical applications (for example, contaminated air treatment in solvent evaporation processes) the gas streams contain mixtures of VOCs of variable composition. It has been reported that the oxidation of a VOC in a mixture differs from its single oxidation due to the interaction of the different species with the catalyst. Santos et al. [16] observed mutual inhibitory effects between ethanol and toluene over TiO_2-supported noble metal catalysts. Tsou et al. [17] studied the oxidation of *o*-xylene and methyl-isobutyl-ketone over Pt-catalysts, observing an inhibitory effect of *o*-xylene on methyl-isobutyl-ketone, due to a competition on the active sites. Kim and Shim [18] observed a mutual inhibitory effect between toluene and benzene over a Ca/Mn_3O_4 catalyst. They suggest that the reaction was a competitive one running on the same active sites. On the other hand, a promoting effect could be due to the exothermic character of the complete oxidation reaction, which locally raises the surface temperature of the catalyst [19].

The rheological properties of clays and clay minerals are ideal raw materials for preparing structured supports and catalysts [20–22] being a better alternative to metallic ones. However, most of the work performed in ceramic monoliths deals with the ceramic called "cordierite" [23, 24]. Nevertheless, the processing of cordierite is high energy demand. The abundance of natural clay and its low cost are likely to make it a strong candidate as catalysts support. A series of bentonite resources are located in Northern Patagonia, Argentina. These resources extend over an area of 94,000 km^2 and constitute 80 % of the country's yearly production of bentonites. Reserve estimation is about 3,500,000 tons. They are mainly sodium bentonites and mixtures Na/Ca [25].

The aim of this work is to study the catalytic behavior of a catalyst based on a manganese oxide or platinum supported on bentonite based monoliths in the combustion of two VOCs (ethanol and toluene) generally found in emissions of the printing industries [26, 27]. The catalytic performance in the oxidation of the VOCs separately and in binary mixture was evaluated.

Experimental

Monoliths preparation

A natural bentonite (90 wt% montmorillonite) from North Patagonia, Argentina, was used. Its percent chemical composition, given by the supplier was SiO_2: 58.0, Al_2O_3: 20.1, MgO: 2.66, CaO: 0.77, Fe_2O_3: 5.88, Na_2O: 2.28, K_2O: 0.01, TiO_2: 0.55, MnO: 0.01 and 8.0 of undetermined ashes (mass contents for the dry sample).

A clay (Tincar Super, Piedra Grande, Argentine) and gibbsite, $Al(OH)_3$ (Alcan) were aggregated to the bentonite.

Extrusion of bentonite dough was performed on a UNICERAM Groupe Mirovide studer, with a water content of 8 wt%. The paste was dried 48 h at room temperature and finally heated at 800 °C for 2 h in an electric furnace in air atmosphere.

The characteristics of the elaborated monoliths were: Shape of cells: triangular, Cell density: 3.1 cells cm^{-2}; Cell dimension: 0.2 cm^2 (0.4 × 0.5); Wall thickness: 0.15 cm; Catalyst block dimension: 1.8 cm diameter, 2 cm high; Open area: 1.4 cm^2.

Catalyst preparation

The preparation of supported catalysts was carried out as follows:

Pt/B Bentonite monoliths were immersed in an aqueous solution of $H_2PtCl_6 \cdot H_2O$ 0.02 M, inside a closed vessel and put through to mechanical orbital agitation for 60 min. Subsequently, the monoliths were washed with deionized water to remove chloride, dried overnight at 100 °C, and calcined at 500 °C for 2 h.

Mn/B The impregnation of the monoliths was carried out in two stages according to Ref. [28]: first, the monoliths were immersed in 100 ml of a 1 M aqueous solution of $Mn(NO_3)_2$ and kept under agitation for 60 min. Then monoliths were dried at 100 °C for 4 h. After this stage, monoliths were immersed in a 0.66 M aqueous solution of $KMnO_4$. After agitation for 60 min, the impregnated monoliths were dried at 100 °C for 4 h and finally calcined at 500 °C for 2 h.

Pt/Mn/B Mn/B monoliths, after having been calcined at 500 °C, were impregnated with $H_2PtCl_6 \cdot H_2O$ 0.02 M in the same way as the Pt/B monoliths. After impregnation, the monoliths were dried overnight at 100 °C and calcined at 500 °C for 2 h.

Catalyst characterization

Manganese and platinum contents were measured by atomic absorption spectroscopy with a Varian AA 240 instrument after dissolving previously crushed and milling monoliths with $HF–HNO_3–HCl$ mixture.

The Brunauer–Emmett–Teller (BET) surface areas, total pore volume, and average pore diameter of the samples were measured by N_2 adsorption at liquid

nitrogen temperature (77 K) in a Micromeritics ASAP 2000 sorptometer. The experiments were performed over small pieces of crushed monoliths.

The surface morphology of the monoliths was studied by scanning electron microscopy (SEM) using a Philips SEM 505 microscope. The experiments were performed over small pieces of crushed monoliths.

The samples were characterized by X-ray diffraction (XRD) methods using a Philips diffractometer in powder form (previously ground monolith). The diffraction patterns were recorded at room temperature from 5° to 70° of 2θ using Cu K$_\alpha$ ($\lambda = 1.5406$ Å) radiation at 0.02 min^{-1} scanning speed and a counting time of 2 s per step.

X-ray photoelectron spectra (XPS) of the compounds in powder form (previously ground monolith) were obtained using a multitechnique system, with a Mg X-ray source and a hemispherical PHOIBOS 150 analyzer operating in the fixed analyzer transmission mode. Binding energies (BE: ±0.1 eV) were calculated using adventitious hydrocarbon (C 1s = 284.6 eV) as the internal reference. Curve fitting was performed with the CasaXPS software.

Temperature programmed reduction (TPR) experiments were performed in Quantachrome equipment Quantasorb Jr., using 25–50 mg of sample in powder form (previously ground monolith). In all cases, the temperature was increased from ambient to 900 °C at a heating rate of 10 °C min^{-1}. A gas mixture of H$_2$–N$_2$, 5 % by volume was used as reducing gas, at a total flow rate of 22 cm^3 min^{-1}. Copper oxide was used for the calibration of the equipment. Quantification of the TPR results was performed assuming that at the end of the experiments all Mn is as MnO.

The acidity of the samples was measured in a Metrohm 794 Basic Titrino with interchanged unity 806 and a Metrohm electrode. A representative 0.50 g sample in powder form was suspended in 45 ml of acetonitrile solution and allowed 3 h in agitation to come to stabilization. This suspension was then titrated with 0.025 N n-butylamine solution.

The adherence of the coatings was evaluated in terms of the weight loss after exposure of the monoliths to ultrasounds. The impregnated monoliths were immersed in 25 ml petroleum ether, inside a sealed beaker, and then treated in an ultrasound bath for 30 min, in a TESTLAB TB10 at 400 W and 40 kHz. After that, the monoliths were dried at 100 °C for 2 h. The weight loss (in wt%) was determined by measuring the weight of the samples both before and after the ultrasonic treatment.

Catalytic oxidation

The catalytic activity of the prepared monoliths was measured for the complete oxidation of ethanol and toluene, individually and in binary mixture. Complete oxidation reactions were carried out at atmospheric pressure in a stainless steel tubular fixed-bed reactor of 45 cm high and 2.3 cm in inner diameter. A feed gas with a VOC concentration of 1,000 mgC m^{-3} in air and a total flow of 1,000 cm^3 min^{-1} (GHSV = 12,000 h^{-1}) was passed through the monolith placed on the top of a carborundum bed. This configuration was designed to premix and preheat the stream entering the reactor, to obtain a homogeneous temperature at the

monolith inlet, measured by a thermocouple placed just at the entrance of the monolith. The reactor was surrounded by an electrical furnace equipped with three independent temperature programmers. The ignition curves were obtained over the range 100–450 °C in incremental steps (25 °C) and the reaction temperature was measured by a thermocouple placed in the middle of the monolith. The data were obtained in steady state. Monoliths were treated under 1,000 cm^3 min^{-1} of air at 450 °C for 1 h before reaction, and then cooled down in air to the starting reaction temperature. The conversion was calculated by measuring VOC disappearance by gas chromatography (Shimadzu GC9A), together with the CO_2 measurement by an on-line IR detector (Telaire T6613). The yield to CO_2 was calculated as the ratio between the CO_2 concentrations divided by its value measured when complete conversion at high temperature had been reached. No partial oxidation products were detected in the combustion of toluene. In the case of ethanol oxidation, the acetaldehyde yield was calculated as moles of ethanol converted to acetaldehyde divided by the moles of ethanol fed into the reactor. In the oxidation of the binary VOC mixture, the feed composition was kept at 1,000 mgC m^{-3}.

Results

Catalyst characterization

The platinum content in the monoliths, determined by atomic spectroscopy, was 0.22 wt% for Pt/B and 0.23 wt% for Pt/Mn/B. The manganese content was 2.0 wt% for Mn/B and 1.9 wt% for Pt/Mn/B.

Table 1 lists the results of nitrogen physisorption obtained for the supported catalysts. The BET surface area of the support was 53 m^2 g^{-1}. After platinum impregnation, the surface area decreased significantly to 35 m^2 g^{-1}. This decrease in the BET surface area upon Pt impregnation is attributed to a fraction of platinum crystallites blocking the smaller pores of the support and thereby increasing the average pore radius from 124 to 167 Å. Impregnation of the bentonite support with manganese does not significantly change the textural properties. The addition of Pt to Mn/B has no effect on the specific area.

**Table 1** Textural properties and XPS results of monoliths

Catalyst	S_{BET} (m^2 g^{-1})	V_p (cm^3 g^{-1})	D_p (Å)	Weight loss (%)	Mn 2p$_{3/2}$ (eV)	Pt 4d$_{5/2}$ (eV)
B	53	0.16	124	0.98		
Pt/B	35	0.15	167	0.99		315.2
						318.4
Mn/B	57	0.16	115	1.1	641.1 (58 %)	
					643.1 (42 %)	
Pt/Mn/B	58	0.15	75	0.98	641.7 (80 %)	317.1
					644.9 (20 %)	

SEM micrographs of catalysts are shown in Fig. 1a–d. It can be seen that the solid Pt/B (Fig. 1b) has a morphology similar to that of the support (Fig. 1a), while the solid Mn/B and Pt/Mn/B (Fig. 1c, d) shows a cluster of small surface particles on the support matrix. In the Mn/B catalyst, the MnO_x layer is deposited on the support surface changing its morphology.

The adherence of catalyst after the ultrasound test showed an approximately 1 wt% weight lost (Table 1).

The XRD patterns of the samples are shown in Fig. 2. The diffraction pattern of the support shows the diffraction lines corresponding to the support, Al_2O_3 and bentonite. Mn/B, Pt/B and Pt/Mn/B samples present the diffraction lines of the support. Manganese oxides were not detected in Mn/B or in Pt/Mn/B catalysts. Metallic Pt or platinum oxides were neither detected in the samples containing platinum.

In the XPS studies, the energy regions of Mn $2p_{3/2}$ and Pt $4d_{5/2}$ core levels were recorded. Although the most intense photoemission lines of platinum were those
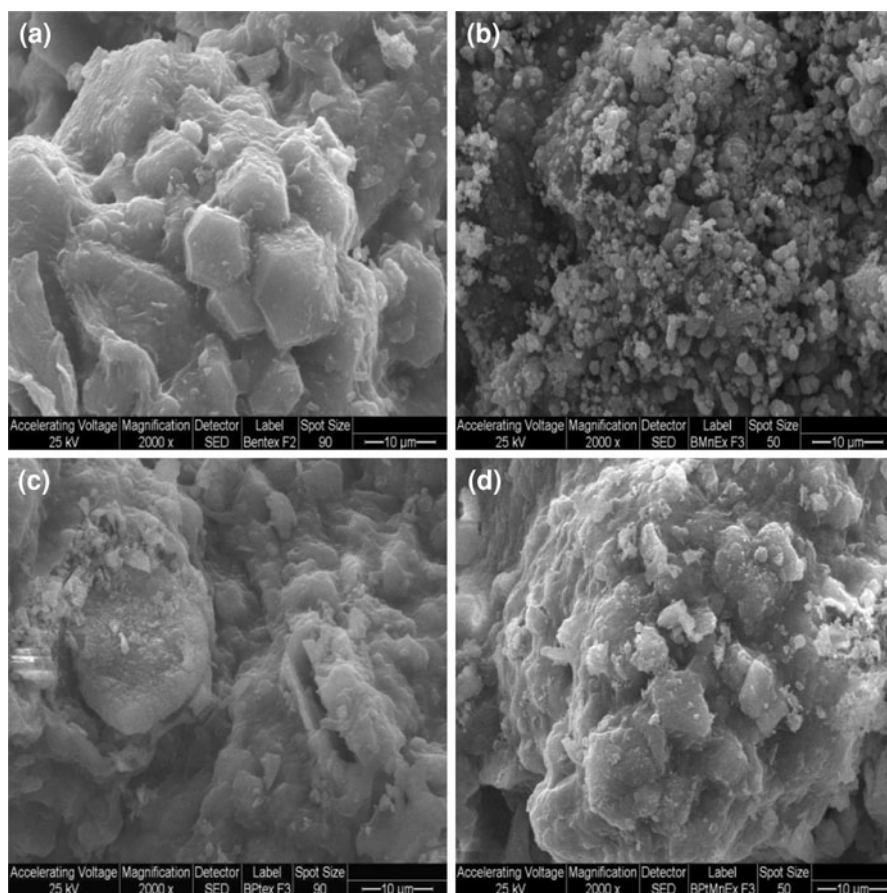
**Fig. 1** SEM micrographs of monoliths, **a** bentonite, **b** Mn/B, **c** Pt/B and **d** Pt/Mn/B
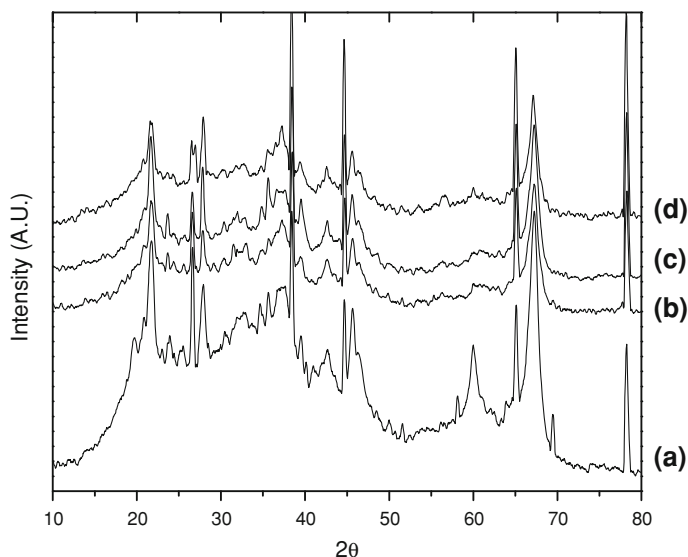
Fig. 2 X-ray diffraction patterns of samples: (*a*) bentonite, (*b*) Mn/B, (*c*) Pt/B and (*d*) Pt/Mn/B

arising from the Pt 4f levels, this energy region was overshadowed by the presence of a very strong Al 2p peak, and thus the Pt 4d lines were analyzed instead [29]. The spectra of Mn $2p_{3/2}$ for Mn/B and Pt/Mn/B monoliths are presented in Fig. 3a and the Mn $2p_{3/2}$ binding energies are also presented in Table 1. For both catalysts, Mn/B and Pt/Mn/B, the Mn $2p_{3/2}$ spectral shape could be reproduced with two Mn $2p_{3/2}$ components assigned to Mn^{3+} and Mn^{4+} [30]. Nevertheless, the addition of platinum to manganese oxide increased the Mn^{3+}/Mn^{4+} ratio remarkably.

The spectra of Pt $4d_{5/2}$ are presented in Fig. 3b. The Pt/B sample showed an asymmetric broad Pt $4d_{5/2}$ peak that could be resolved, after curve fitting procedures, into two components with binding energies of 318.4 and 315.2 eV. The component at higher binding energy can be ascribed to PtO_2 species [29, 31], whereas the second band at lower binding energy can be assigned to the presence of Pt(II) species [32]. Pt/Mn/B monoliths showed a Pt $4d_{5/2}$ peak that the curve fitting give just one component at 317.1 eV assigned to PtO_2 [31].

The reduction behavior of Pt/B, Mn/B and Pt/Mn/B catalysts was followed by H_2-TPR, as shown in Fig. 4. In Mn/B monolith, a shoulder at lower temperature (310 °C) is related to the reduction of highly dispersed MnO_x species [33–35]. Additionally, two reduction peaks centered at 409 and 495 °C are observed. The first reduction peak corresponded to the combined reduction of MnO_2 or Mn_2O_3 to Mn_3O_4 [36], and the second reduction peak could represents the reduction of Mn_3O_4 to MnO [36] or the reduction of Mn_5O_8 to MnO [37]. Furthermore, the TPR pattern reveals a peak at about 680 °C, which could be associated to the reduction of Mn^{3+} to Mn^{2+} ions incorporated in the support lattice [35, 38]. Platinum in the mixed manganese oxide/platinum catalyst significantly affects the reduction behavior of the oxide. The TPR-profile changes in several ways: the shape of the curves, the
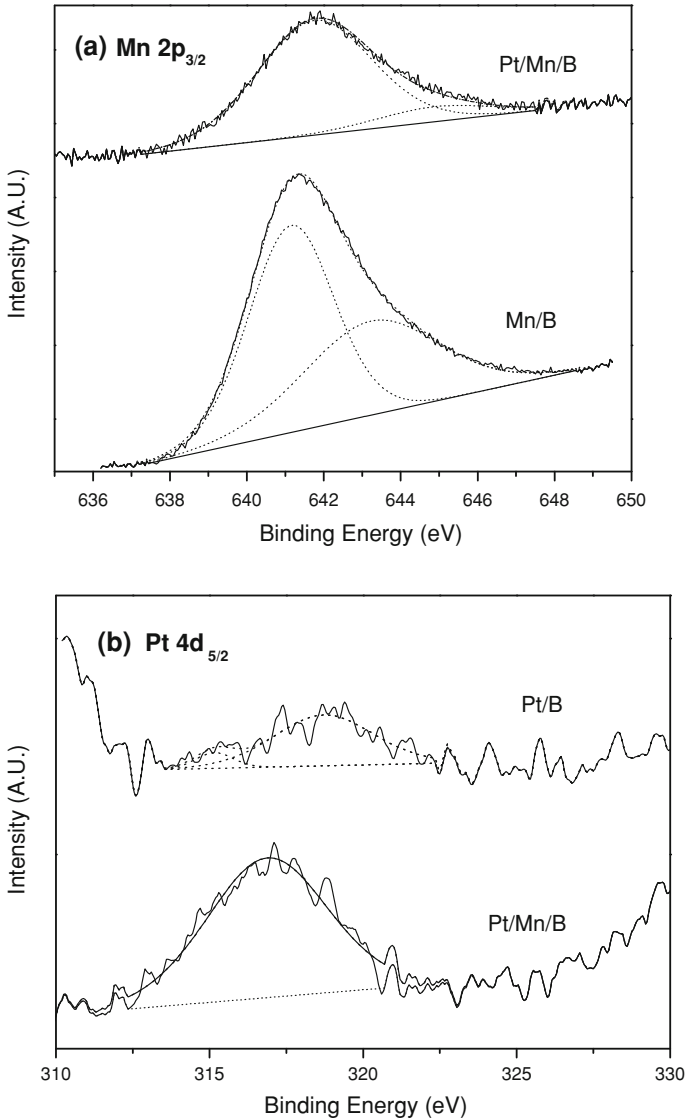
Fig. 3 Mn $2p_{3/2}$ (**a**) and Pt $4d_{5/2}$ (**b**) XPS spectra of samples

number of peaks, the reduction rate and temperature. A possible explanation for that could be that platinum and manganese are in intimate contact and therefore can affect each other by the spillover of hydrogen atoms from platinum to manganese or by nucleation of hydrogen molecules to atoms by platinum making the hydrogen more reactive [39, 40].

From the TPR results, the calculated average oxidation state of Mn was 3.62 for Mn/B and 3.60 for Pt/Mn/B. This effect was observed by another author [41].
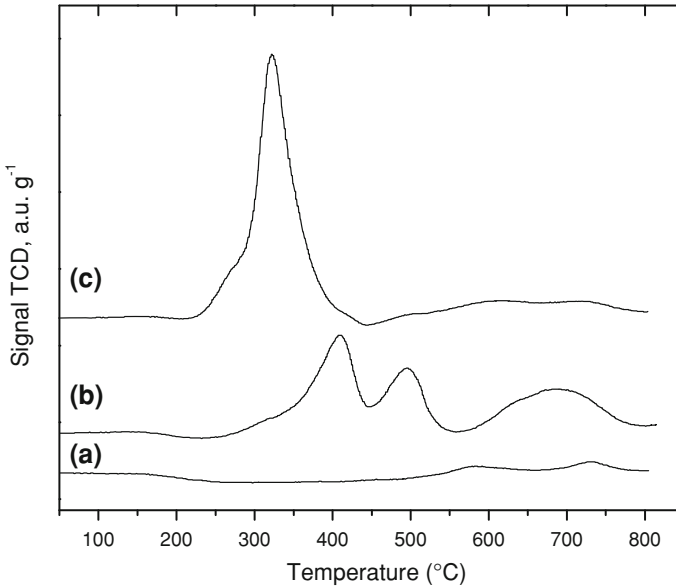
**Fig. 4** TPR profiles of samples: (*a*) Pt/B; (*b*)Mn/B and (*c*) Pt/Mn/B

Catalytic activity

*Catalytic oxidation of individual compounds*

The catalytic activity of supported Pt, Mn and Pt/Mn bentonite monoliths towards the oxidation of each VOC, ethanol and toluene, is presented in Fig. 5. For comparison, the activity of the bentonite support is also presented. Additionally, the temperatures for 10, 50 and 90 % conversion into CO_2 are listed in Table 2. In the three catalysts, ethanol is more easily oxidized than toluene, in accordance with other authors [42, 43].

The addition of Pt to Mn greatly improves the oxidation of ethanol, lowering the T_{50} and T_{90} to about 40 and 30 °C, respectively.

On the other hand, the activity towards ethanol oxidation of both catalysts containing platinum, Pt/Mn/B and Pt/B, is rather similar, the bimetallic catalyst being a little more active at temperatures above 200 °C. In fact, the T_{90} of Pt/Mn/B monolith is 10 °C lower than that of Pt/B.

Apart from CO_2 and H_2O, a product of ethanol incomplete oxidation (acetaldehyde) was detected. As was observed in previous work [44], the oxidation of ethanol may run according to the following scheme:

Acetaldehyde

Ethanol $\longrightarrow$ $CO_2 + H_2O$
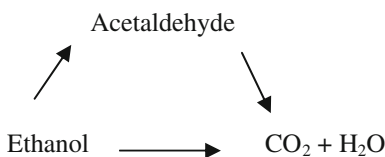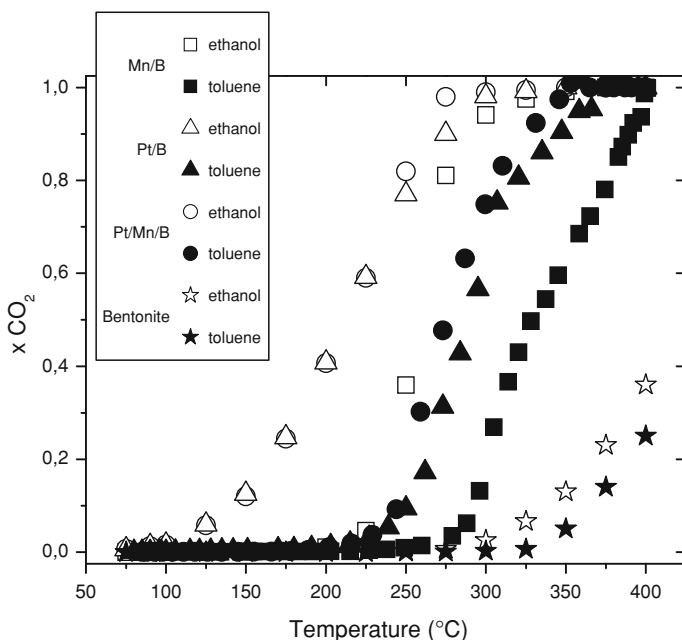
Fig. 5 Ethanol and toluene ignition curves over monoliths

Table 2 Catalytic activity of pure compounds expressed as T_{10}, T_{50} and T_{90} (°C) (temperatures at CO_2 conversion of 10, 50 and 90 %)

Catalyst	Ethanol			Toluene		
	T_{10}	T_{50}	T_{90}	T_{10}	T_{50}	T_{90}
Mn/B	229	256	294	292	327	389
Pt/B	145	212	278	254	288	349
Pt/Mn/B	145	212	265	244	276	324

Fig. 6 shows the production of acetaldehyde as a function of the reaction temperature. Although the aldehyde is the most abundant intermediate, acetaldehyde yield did not exceed 6 % for Pt/Mn/B and 3 % for Pt/B. For Mn/B the acetaldehyde yield is negligible. The maximum of acetaldehyde occurs at around 200 and 225 °C for Pt/Mn/B and Pt/B, respectively.

As can be seen in Fig. 5 and Table 2, the activity towards toluene oxidation markedly decreases in the order of Pt/Mn/B > Pt/B > Mn/B. As in the case of ethanol oxidation, the addition of Pt to Mn enhanced toluene conversion, lowering the T_{50} and T_{90} to about 50 and 60 °C, respectively. On the other hand, no partial oxidation products were detected in toluene oxidation.

In accord with the TPR results, the reduction of the Mn/B catalyst occurs at higher temperatures than in Pt/Mn/B, and consequently the oxidation of VOCs on the Mn/B catalyst was more difficult than that on the Pt/Mn/B catalyst. It may be
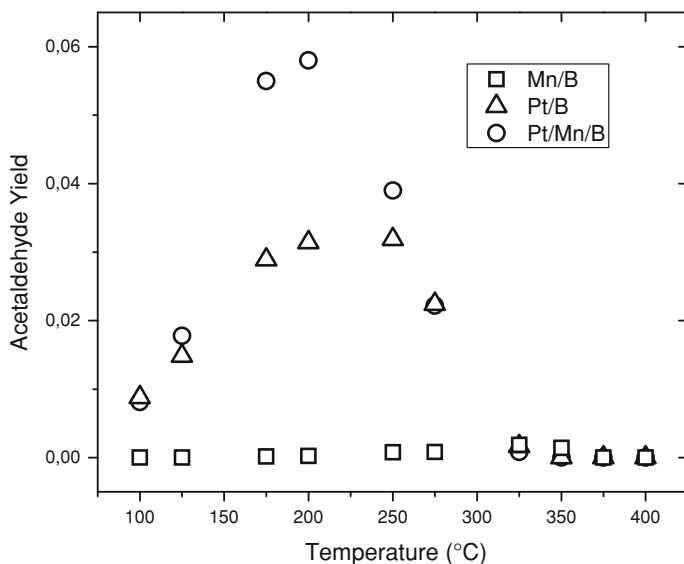
**Fig. 6** Evolution of acetaldehyde yield with reaction temperature

assumed that the higher activity for the bimetallic catalysts resulted from the valence state as well as the favorable synergetic effects between Pt and Mn.

It has been reported that the activity towards the oxidation of VOCs of manganese oxide-based catalysts is related to the presence of the Mn^{3+}–Mn^{4+} redox couple [45, 46]. As we observed in XPS experiments, the Mn^{3+}/Mn^{4+} surface ratio increases when Pt is added to Mn. In previous work [47], in the oxidation of ethanol on manganese oxides prepared from $KMnO_4$ and $Mn(NO_3)_2$, we assumed that a high concentration of Mn^{3+} could originate a weak Mn–O bond and the formation of more active oxygen species in the lattice, which would improve H subtraction from the adsorbed alcohol molecule. Although the combustion of ethanol is independent of the presence of Mn, the synergetic effect of Pt–Mn is important when toluene is analyzed. The temperatures T_{10}, T_{50} and T_{90} on Pt/Mn/B are lower than that of Pt/B. These results are similar to that reported by Sanz et al. [48]. The authors have shown that "Pt improved the catalytic activity of MnO_x decreasing the complete toluene oxidation temperature from 300 to 265 °C (25 °C in this work)". In our opinion, this result demonstrates that Pt and the presence of Mn^{3+}/Mn^{4+} redox couple is crucial.

The acidity of the samples was evaluated by titration with *n*-butylamine. Results are presented in Fig. 7. Taking into account the acidity properties of the samples, the support has no effect on the reaction. Additionally, toluene conversion depends on the acidity of the samples, the more the acidity of the samples the more the toluene conversion.

Acetaldehyde formation could be associated to an interaction between the OH of the ethanol and a Pt site of the solid.

The Pt–Mn interaction in Pt/Mn/B monolith could be results in a mayor acetaldehyde formation. The increased acidity in Pt/Mn/B sample originates an
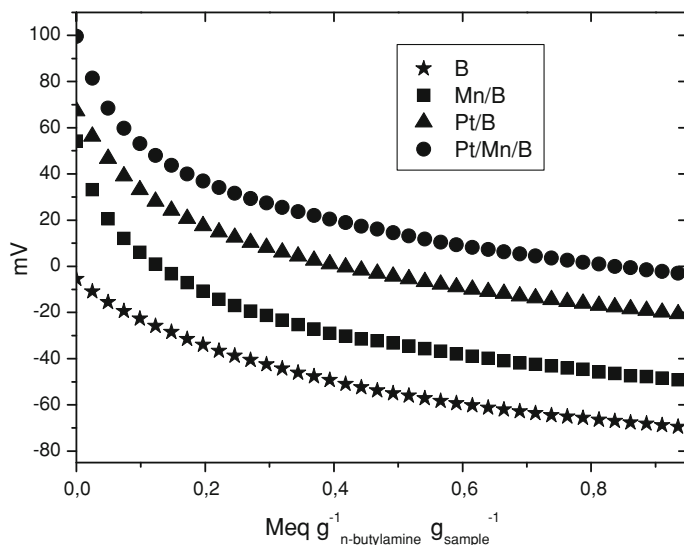
Fig. 7 Titration of samples with *n*-butylamine

increased donor character of ethanol, a phenomenon that results in the formation of adsorbed inactive spectators according with Peluso et al. [28].

Nevertheless, the higher catalytic activity of the Pt/Mn/B monolith could be associated to an increase in the amount of surface Mn^{3+} species, resulting in a higher capacity of combustion of adsorbed intermediate species [47].

The Pt/Mn/B monolith presents a promissory activity in the combustion of VOCs. Working at a GHSV of 12,000 h^{-1}, a T_{90} of 265 and 324 °C is obtained for ethanol and toluene, respectively. Burgos et al. [19] oxidized toluene over cylindrical $Pt/Al_2O_3/Al$ monoliths (330 cpi, 6 cm^3 volume) at lower temperature but working at a GHSV of 3,680 h^{-1}. Morales et al. [34] obtained a T_{90} of 210 and 300 °C for ethanol and toluene, respectively, over MnCu supported on 330 cpi cylindrical Fecralloy monoliths working at a GHSV of 3,000 h^{-1}. Li et al. [49] studied the combustion of toluene over 0.2 %Pd–6 %$Ce_xLa_{1-x}O_2$ supported on 200 cpi cordierite monoliths (48 × 24 × 40 mm^3) working at 0.3 $m^3 h^{-1}$, obtained 90 % toluene conversion at 230 °C. Monoliths prepared in this work are easy to obtain and are ready made to incorporate the active phase directly by wet impregnation.

Ethanol–toluene binary mixture

The activity of the monoliths in a mixture of ethanol and toluene (with the same total concentration as in the individual compounds) was also investigated. Fig. 8a shows the results of the total combustion to CO_2. It can be observed that Pt/Mn/B presents the highest initial activity towards the combustion of the VOC mixture; however, the three catalysts achieve complete oxidation to CO_2 at almost 350 °C.

Fig. 8b presents the conversion of ethanol and toluene in the mixture. For the three catalysts, ethanol again was more easily oxidized than toluene. The performance of the monoliths for the combustion of the two VOCs, ethanol and toluene, follows the order: Pt/Mn/B > Pt/B > Mn/B. The same order of activity was found in the oxidation of toluene alone. In the oxidation of ethanol alone, Pt/Mn/B presented similar activity to that of Pt/B at temperatures below 200 °C, being more active at higher temperatures. In the VOCs mixture, Pt/Mn/B is more active than Pt/B even at low temperatures.
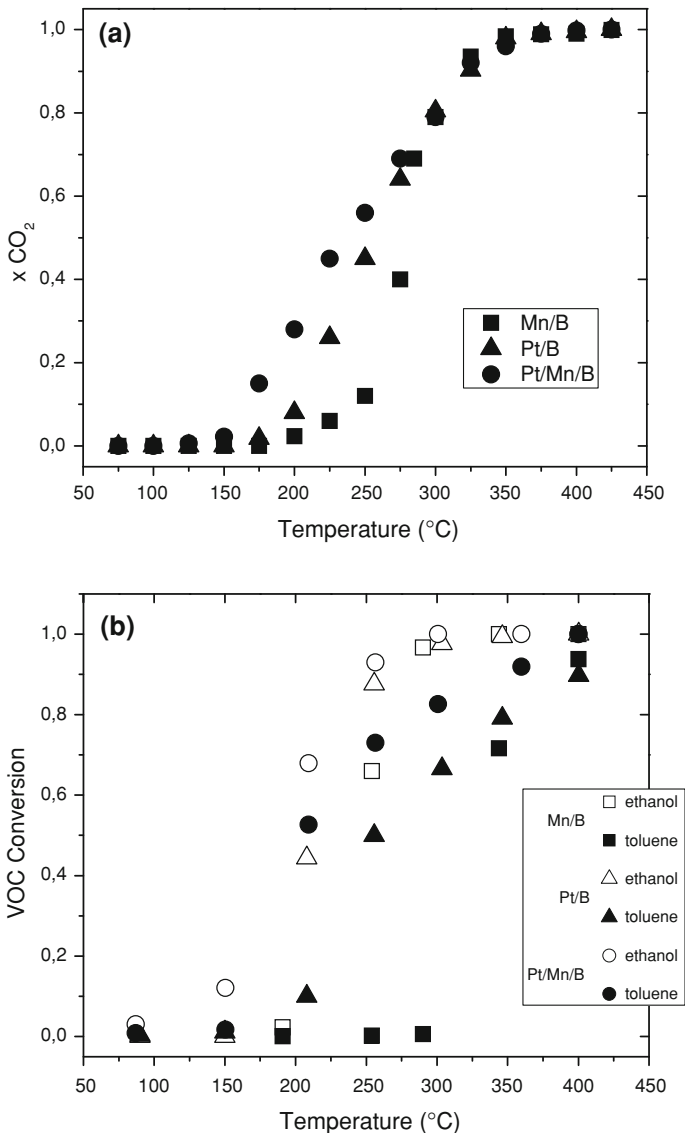

Fig. 8 Total conversion (a) and partial conversion (b) of ethanol and toluene in the VOC mixture

The least active monolith, Mn/B, presents a high activity towards ethanol oxidation, whereas toluene oxidation starts when almost complete ethanol conversion has been obtained at about 290 °C.

Taking into account the formation of intermediate products, the presence of toluene modified the selectivity of ethanol to acetaldehyde. Fig. 9 shows the acetaldehyde yield as a function of the reaction temperature in the ethanol–toluene mixture. For the three monoliths, the curves of ethanol conversion to acetaldehyde are shifted to higher temperatures. This effect was also observed by other authors [19, 50]. Additionally, higher values of maximum acetaldehyde yield are observed, especially in Mn/B monolith. Agüero et al. [51] have found that the presence of toluene increases the acetaldehyde yield in the combustion of the ethanol–toluene mixture over an alumina-supported manganese oxide.

According to different authors [52–54], the total oxidation of toluene occurs when the molecule is adsorbed in parallel to the surface. Our previous results [44] have shown that the adsorption–oxidation of ethanol occurs on two sites: (i) terminal oxygen and (ii) OH groups formed from Mn^{4+} vacancies. These results allow us to suggest that the toluene adsorption blocks the catalytic sites where ethanol can be oxidized directly to CO_2. Then, the acetaldehyde formation is more favorable.

The presence of ethanol enhanced toluene oxidation, especially in the catalyst containing platinum. The T_{50} decreased from 276 to 207 °C and 291 to 256 °C in Pt/Mn/B and Pt/B, respectively, when toluene was oxidized alone and in the mixture with ethanol. This effect is most probably a consequence of the higher exothermicity of the process when the mixtures are considered, as was reported by other authors in ethanol–toluene mixtures [43, 50].
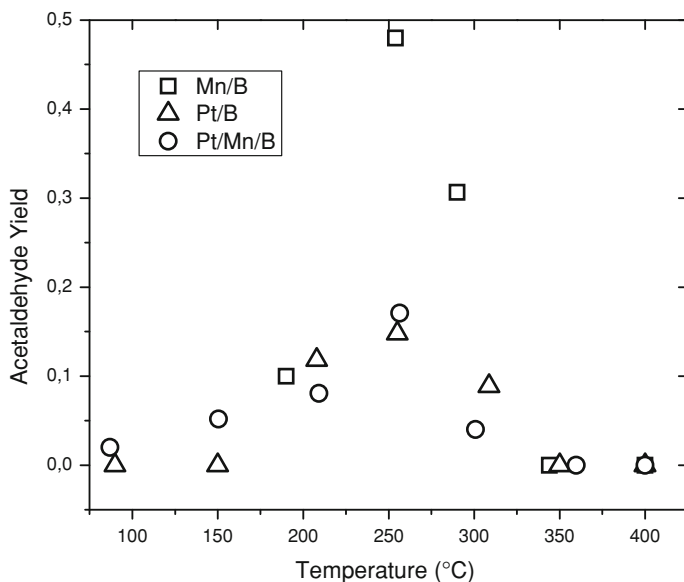
Fig. 9 Evolution of acetaldehyde yield with reaction temperature in the ethanol–toluene mixture

The studies carried out in this work demonstrated that the Pt/MnO$_x$ active phase supported on bentonite monolith is a promising catalyst for VOCs abatement. Further investigation in different shapes and different materials for monolith supports is currently being carried out in our laboratory.

Conclusions

Ceramic monoliths using natural bentonites as raw materials were prepared. The relatively high surface area of the support allows the incorporation of the active phases (Mn, Pt and Pt/Mn) directly by wet impregnation. The impregnated phases show excellent adhesion to the monoliths. The XRD analyses shows only the diffraction peaks of the support and no metallic platinum or manganese oxides phases were detected. The addition of Pt to Mn increases the surface Mn^{3+}/Mn^{4+} ratio in comparison to Mn/B and facilitates the reduction of the manganese oxide phases. The acidity of the samples decrease in the order: Pt/Mn/B > Pt/B > Mn/B > B.

The catalytic activity in toluene oxidation was in the order Pt/Mn/B > Pt/B > Mn/B > B. In ethanol oxidation, the conversion order was: Pt/Mn/B = Pt/B > Mn/B > B. Although the combustion of ethanol is independent of the presence of Mn, a favorable synergetic effect between Pt and Mn is important when toluene is analyzed, together with the increase in the surface Mn^{3+}/Mn^{4+} ratio, and the increase in the catalysts acidity.

In the VOC mixture, the presence of toluene shifts the curve of ethanol oxidation towards acetaldehyde to higher temperatures. On the other hand, the presence of ethanol has a promoting effect on toluene oxidation, attributed to a local heating effect.

References

1. Horsley JA (1993) Catalytica environmental report no. E4. Catalytica Studies Division, Mountain View
2. Spivey J (1987) Ind Eng Chem Res 26:2165–2180
3. Armor JN (1992) Appl Catal B 1:221–256
4. Hermia J, Vigneron S (1993) Catal Today 17:349–358
5. Jin L, He M, Lu J, Luo M, Gao L, He J (2008) J Rare Earths 26:614–618
6. Saqer S, Kondarides D, Verykios X (2009) Top Catal 52:517
7. Lamonier JF, Boutoundou A, Boutoundou C, Perez-Zurita M, Siffert S, Aboukais A (2007) Catal Lett 118:165–172
8. Jiratova K, Mikulova J, Klempa J, Grygar T, Bastl Z, Kovanda F (2009) Appl Catal A 361:106–116
9. Palacio L, Velasquez J, Echavarria A, Faro A, Ribeiro F, Ribeiro M (2010) J Hazard Mater 177:407–413
10. Lu H, Zhou Y, Huang H, Zhang B, Chen Y (2011) J Rare Earths 29:855–860
11. Avila P, Montes M, Miro EE (2005) Chem Eng J 109:11–36
12. Agüero F, Barbero B, Costa-Almeida L, Montes M, Cadus L (2011) Chem Eng J 166:218–223
13. Gatica J, Vidal H (2010) J Hazard Mater 181:9–18

14. Dominguez M, Barrio I, Sanchez M, Centeno M, Montes M, Odriozola J (2008) Catal Today 133: 467–474
15. Barrio I, Legorburu I, Montes M, Dominguez M, Centeno M, Odriozola J (2005) Catal Lett 101: 151–157
16. Santos V, Carabineiro S, Tavares P, Pereira M, Orfao J, Figueiredo J (2010) Appl Catal B 99: 198–205
17. Tsou J, Magnoux P, Guisnet M, Orfao J, Figueiredo J (2005) Appl Catal B 57:117–123
18. Kim S, Shim W (2010) Appl Catal B 98:180–185
19. Burgos N, Paulis M, Mirari Antxustegi M, Montes M (2002) Appl Catal B 38:251–258
20. Benbow J, Bridgwater J (1993) Paste flow and extrusion. Clarendon Press, Oxford
21. Graczyk J, Gleissie W (1990) Petrochimie 43:27–30
22. Komova O, Simakov A, Kovalenko G, Rudina N, Chuenko T, Kulikovskaya N (2007) Kinet Catal 48:803–811
23. Forzatti P, Ballardini D, Sighicelli L (1998) Catal Today 41:87–94
24. Williams JL (2001) Catal Today 69:3–9
25. Lombardi B, Baschini M, Torres Sanchez R (2003) Appl Clay Sci 22:309–312
26. Kiurski J, Branislav M, Adamovic D, Mihailovic A, Grujic S, Oros I, Krstc J (2012) Renew Sust Energy Rev 16:660–667
27. Wolf M (1994) Stud Environ Sci 61:29–34
28. Peluso MA, Pronsato E, Sambet JE, Thomas HJ, Busca G (2008) Appl Catal B 78:73–79
29. Serrano-Ruiz J, Huber G, Sánchez-Castillo M, Dumesic J, Rodríguez-Reinoso F, Sepúlveda-Escribano A (2006) J Catal 241:378–388
30. Ponce S, Peña M, Fierro J (2000) Appl Catal B 24:193–205
31. Serre C, Garin F, Belot G, Maire G (1993) J Catal 141:1–8
32. Shyu J, Otto K (1998) Appl Surf Sci 32:246–252
33. Liu X, Lu J, Qian K, Huang W, Luo M (2009) J Rare Earths 27(418):424
34. Morales M, Barbero B, Lopez T, Moreno A, Cadús L (2009) Fuel 88:2122–2129
35. Trawczynski J, Bielak B, Mista W (2005) Appl Catal B 55:277–285
36. Kapteijn F, Van Langeveld A, Moulijn J, Andreini A, Vuuman M, Turek A, Jehng J, Wachs I (1994) J Catal 150:94–104
37. Mirzaei A, Shaterian H, Habibi M, Hutchings G, Taylor S (2003) Appl Catal A 253:499–508
38. Dobber D, Kiebling D, Schmitz W, Wendt G (2004) Appl Catal B 52:135–143
39. Carno J, Ferrandon M, Bjornbom E, Jaras S (1997) Appl Catal A 155:265–281
40. Tang X, Chen J, Huang X, Xu Y, Shen W (2008) Appl Catal B 81:115–121
41. Ayastuy JL, González-Marcos M, González-Velazco J, Gutiérrez-Ortiz M (2007) Appl Catal B 70:532–541
42. O'Malley A, Hodnett B (1999) Catal Today 54:31–38
43. Agüero F, Barbero B, Pereira M, Figueiredo J, Cadus L (2009) Ind Eng Chem Res 48:2795–2800
44. Lamaita L, Peluso MA, Sambeth JE, Thomas HJ (2005) Appl Catal B 61:114–119
45. Suib SL (2008) J Mater Chem 18:1623–1631
46. Peluso MA, Sambeth JE, Thomas HJ (2003) React Kinet Catal Lett 80:241–248
47. Peluso MA, Gambaro L, Pronsato E, Gazzoli D, Thomas HJ, Sambeth JE (2008) Catal Today 133:487–492
48. Sanz O, Delgado J, Navarro P, Arzamendi G, Gandía L, Montes M (2011) Appl Catal B 110:231–237
49. Li T, Lei Y, He Y, Teng B, Luo M, Zhao L (2011) Reac Kinet Mech Cat 103:419–429
50. Santos V, Pereira M, Orfao J, Figueiredo J (2001) J Hazard Mater 185:1236–1240
51. Agüero F, Barbero B, Gambaro L, Cadus L (2009) Appl Catal B 91:108–112
52. Bielanski A, Haber J (1990) Oxygen in catalysis, vol 43. Marcel Dekker, New York
53. Witko M, Haber J, Tokarz R (1993) J Mol Catal 82:457–466
54. Irigoyen B, Juan A, Larrondo S, Amadeo N (2001) J Catal 201:169–182